

# Unveiling the Coupling of Single Metallic Nanoparticles to Whispering-Gallery Microcavities

Yves Auad,\* Cyrille Hamon, Marcel Tencé, Hugo Lourenço-Martins, Vahagn Mkhitarian, Odile Stéphan, F. Javier García de Abajo, Luiz H. G. Tizei, and Mathieu Kociak\*



Cite This: <https://doi.org/10.1021/acs.nanolett.1c03826>



Read Online

ACCESS |



Metrics & More



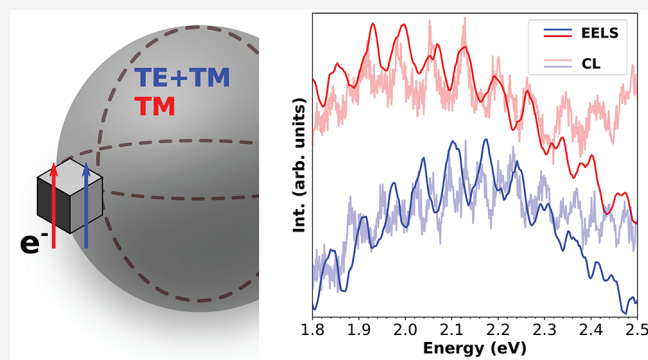
Article Recommendations



Supporting Information

**ABSTRACT:** Whispering-gallery mode resonators host multiple trapped narrow-band circulating optical resonances that find applications in quantum electrodynamics, optomechanics, and sensing. However, the spherical symmetry and low field leakage of dielectric microspheres make it difficult to probe their high-quality optical modes using far-field radiation. Even so, local field enhancement from metallic nanoparticles (MNPs) coupled to the resonators can interface the optical far field and the bounded cavity modes. In this work, we study the interaction between whispering-gallery modes and MNP surface plasmons with nanometric spatial resolution by using electron-beam spectroscopy with a scanning transmission electron microscope. We show that gallery modes are induced over a selective spectral range of the nanoparticle plasmons, and additionally, their polarization can be controlled by the induced dipole moment of the MNP. Our study demonstrates a viable mechanism to effectively excite high-quality-factor whispering-gallery modes and holds potential for applications in optical sensing and light manipulation.

**KEYWORDS:** electron microscopy, electron energy-loss spectroscopy, cathodoluminescence, whispering-gallery modes, metallic nanoparticles



The past few years have witnessed unprecedented advances in photonic technologies. In particular, plasmonics has attained the precise engineering of absorption and scattering properties of metallic nanoparticles due to improvements in synthesis methods.<sup>1–4</sup> At the same time, fabrication techniques have allowed the widespread use of whispering-gallery-mode resonators (WGMRs), which have attracted strong interest in the context of quantum electrodynamics,<sup>5,6</sup> optomechanics,<sup>7,8</sup> and sensing applications.<sup>9,10</sup> The tuning capability of both technologies makes the study of coupled systems particularly interesting, as we discuss throughout this work.

A physical description of WGMRs was first proposed by Lord Rayleigh using acoustic waves circulating the dome of St. Paul's Cathedral,<sup>11</sup> while the electromagnetic-wave analogue can be found in circular or spherical microstructures. Resonances are characterized by their transverse electric (TE) or magnetic (TM) polarization and a set of angular, radial, and azimuthal mode numbers ( $l$ ,  $q$ , and  $m$ ). In addition, WGMRs made from materials with low intrinsic loss, such as silica, can sustain modes that have exceptionally high quality factors<sup>5</sup> ( $Q$  factors).

Due to its high  $Q$  factor, coupling light to a WGMR is a challenging task. Efficient methods almost always rely on evanescent fields using gratings, prisms, or tapered fibers.<sup>12–15</sup> In particular, fiber tapering can reach coupling efficiencies as high as 99% but requires active positioning to maintain this

level of performance over long time periods. Free-space light is an alternative to evanescent coupling, but it has only encountered partial success, with spheres<sup>16,17</sup> and asymmetric cavities<sup>18,19</sup> having high radiative loss due to the bounded nature of the gallery modes.

A practical solution to the problem is to couple an intermediate (e.g., plasmonic) nanoparticle to the gallery modes and to employ it as an evanescent light coupler into the WGM microresonator.<sup>20–23</sup> This approach has been successfully used to detect and characterize the nanoparticle using mode energy shifting,<sup>24–26</sup> splitting,<sup>27,28</sup> or broadening<sup>29,30</sup> of the unperturbed resonances. Single-metallic-nanoparticle and gallery-mode coupling using far-field light has been studied for applications in photocatalysis,<sup>31</sup> as well as for engineering ultranarrow plasmonic resonances.<sup>32,33</sup> Selective coupling into TE and TM modes depending on the incident free-space light polarization has also been observed,<sup>34</sup> finding interesting applications in sensing thanks to the clearer mode

**Received:** October 4, 2021

**Revised:** December 8, 2021

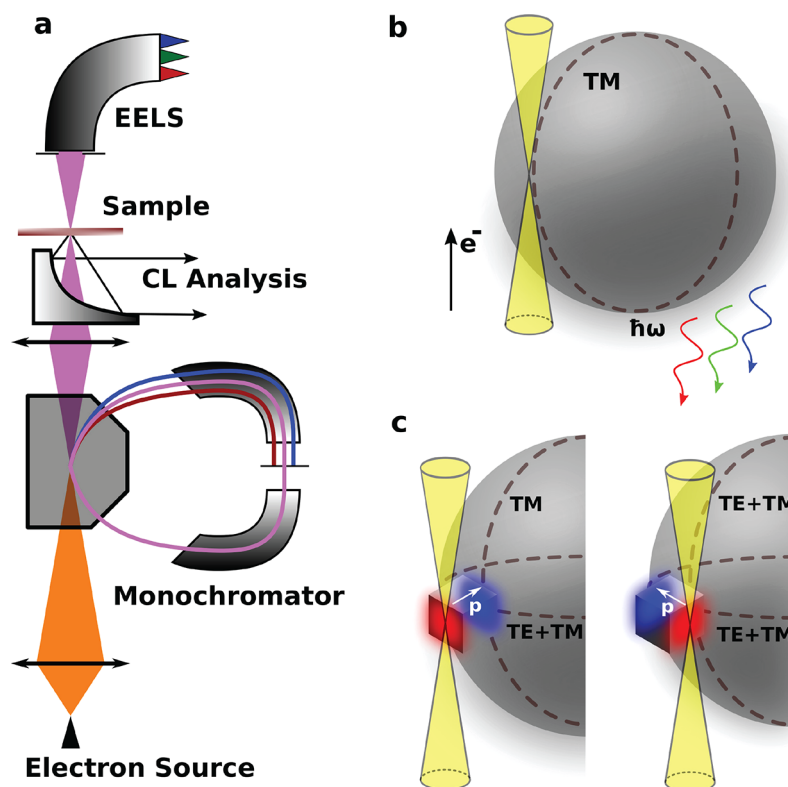


**Figure 1.** Configuration used to study the coupling between a MNP and a WGMR. (a) Scheme of an electron microscope containing an electron source, an electron monochromator, a CL mirror, the sample, and an electron spectrometer. (b) Scheme of an electron beam and the excited TM mode (dashed line) in a bare dielectric sphere. (c) Through the addition of a metallic nanocube, the polarization of the excited WGM can be controlled by the electron-probe position.

identification enabled by this method.<sup>10</sup> However, a sufficient degree of spatial resolution to study the induced near electric field is still lacking in all of the aforementioned studies.

An alternative to study nanoparticles with high spatial resolution is to use a scanning transmission electron microscope (STEM). Electron energy-loss spectroscopy (EELS) and cathodoluminescence (CL) spectroscopy are techniques that can be performed inside the STEM and can combine the sub-nanometer probe size with high spectral resolution (<30 meV) when monochromatic electron sources are used. EELS and CL have been extensively explored to study small (radius <150 nm) particles,<sup>35–37</sup> including the observation of low-order optical modes in SiO<sub>2</sub> spheres by Hyun et al.<sup>38</sup> Large spheres (radius >1.5 μm) have been studied with electron beams using photon-induced near-field electron microscopy,<sup>39</sup> in which a few gallery modes have been observed due to the interaction of an externally applied optical field with the free electrons.<sup>40</sup> More recently, Müller et al. have measured broad-band light emission from high-Q WGMRs using fast electrons,<sup>41</sup> but without the complementary information obtained from EELS. Most of these examples, however, could not resolve a large number of modes. In addition, the bare resonators did not offer much to be spatially explored due to their spherical symmetry.

In this work, we study the coupling of an electron beam to large SiO<sub>2</sub> spheres, in which the narrow-band resonances observed by EELS and CL are attributed to circulating gallery modes in the plane containing the electron trajectory. We explore the coupling of a single silver nanocube with the WGMR through the modulation of the low-Q resonances of the nanocube surface plasmons by the higher-Q gallery modes,

as well as by a dependence of the gallery-mode polarization on the orientation of the electron-induced nanoparticle dipole moment, which can be achieved by changing the electron probe position.<sup>42,43</sup> Figure 1 presents a scheme of the experimental setup, as well as illustrations of the influence of the electron beam position on the excitation of modes with different polarizations.

The analytical solution of the energy loss probability of a fast electron upon interaction with a spherical dielectric body can be written as<sup>44–46</sup>

$$\Gamma_{\text{loss}}(\omega) = \frac{1}{c\omega} \sum_{l=1}^{\infty} \sum_{m=-l}^l K_m^2 \left( \frac{\omega b}{v\gamma} \right) \times [C_{lm}^M \text{Im}(t_l^M) + C_{lm}^E \text{Im}(t_l^E)] \quad (1)$$

where  $K_m$  is a modified Bessel function of order  $m$ ,  $b$  is the electron impact parameter with respect to the sphere center,  $t_l^M$  and  $t_l^E$  are the Mie scattering coefficients,<sup>47–49</sup> which depend exclusively on the sphere radius and its dielectric function, and  $C_{lm}^M$  and  $C_{lm}^E$  are coupling coefficients that depend on the ratio of electron to light velocities,  $v/c$ . The photon emission probability can be written similarly by making the substitution  $\text{Im}\{t_l^{E,M}\} \rightarrow |t_l^{E,M}|^2$ .<sup>44</sup> These simple results show that EELS (CL) is a well-fitted tool to study extinction (scattering) spectroscopy on the nanometer scale, as it is the case in smaller systems.<sup>50</sup>

We have used nonfunctionalized SiO<sub>2</sub> spheres from BangsLabs Inc.<sup>51</sup> ranging from 1.50 to 2.00 μm in radius for the experiments. We used a modified Nion Hermes 200 instrument fitted with an Attolight Mönch CL system. The

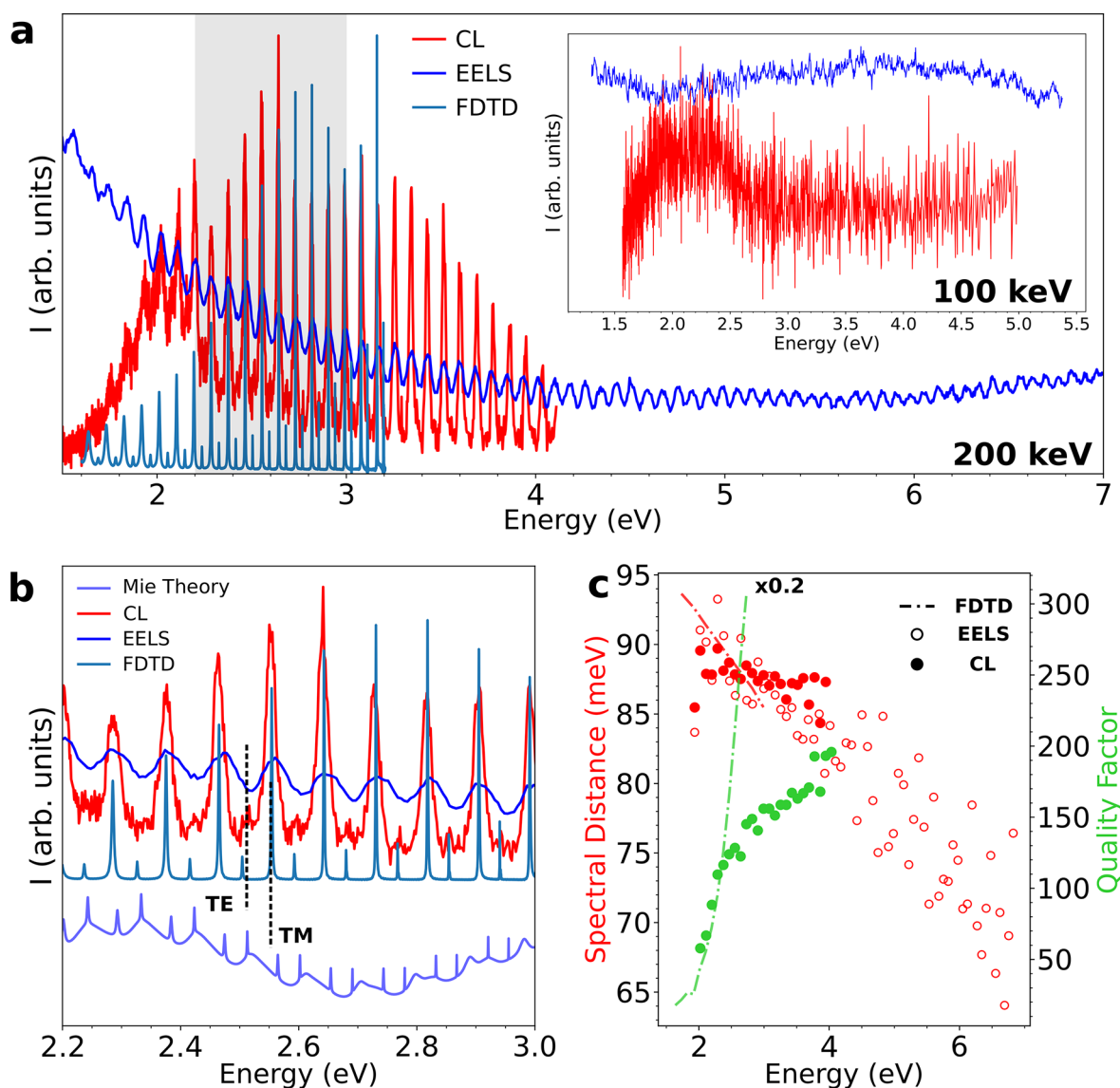


**Figure 2.** Emergence of optical modes in a  $\text{SiO}_2$  sphere of  $1.595 \mu\text{m}$  radius. (a) EELS and CL spectra measured by using 200 keV, compared to FDTD simulations. The inset shows measurements at 100 keV, lacking any visible resonances. (b) Enlarged area around the highlighted gray rectangle in (a). (c) Measured CL and simulated FDTD Q factors, plotted along with the spectral distance from EELS, CL, and FDTD. The FDTD Q factor is divided by a factor of 5 for readability.

monochromatization scheme of the Hermes instrument allows us to reach down to  $\sim 5$  meV spectral resolution and access energies  $>40$  meV at a nominal incident acceleration of 60 kV. This has enabled multiple works in the infrared regime, especially on phonons<sup>52–54</sup> and plasmons.<sup>55,56</sup> However, at higher acceleration energies and with a focus on the relatively high energy losses and broader energy scales as explored in this work, a spectral resolution of 20–30 meV is more appropriate. Experimental results were interpreted by energy-loss simulations done by using a 3D finite-difference time-domain (FDTD) method available in Ansys Lumerical<sup>57</sup> and based on the work from Cao et al.<sup>58</sup> Mie scattering calculations were used to estimate the sphere radius.<sup>49,59</sup> The dispersion values for the  $\text{SiO}_2$  response were taken from Malitson's work.<sup>60</sup>

Figure 2 shows the combined results of EELS and CL measurements using acceleration voltages of 200 and 100 kV for one bare sphere suspended on a carbon membrane of  $\sim 20$  nm thickness. More than 80 resonances were observed in the broad-band excitation using 200 keV electrons in EELS, while

no energy loss was observed for 100 keV due to the reduced coupling for slower electrons. In both the experimental results and the FDTD simulations, TE polarization is poorly excited by the fast electron, also as a consequence of eq 1 due to the smaller coupling strengths of TE in comparison with TM for these electron energies.

Each resonance in EELS and CL was fitted and the obtained center subtracted from the adjacent mode to form a spectral distance curve, which was subsequently compared with the theoretical free spectral range (FSR).<sup>61,62</sup> These values were used for modes from 2.0 to 3.0 eV to extract the effective index of refraction. The index was calculated to be 1.398 at 2.0 eV and 1.409 at 3.0 eV, which are values that agree within  $\sim 95\%$  accuracy with reference values.<sup>60</sup> Beyond 3.0 eV, modes have Q factors exceeding  $10^5$  from Mie theory, which would be easily washed out by losses and finite energy resolution of our experimental setup. This is especially important for the far-UV resonances observed in EELS, as multiple sets of radial orders combined with the limited spectral resolution of the electron

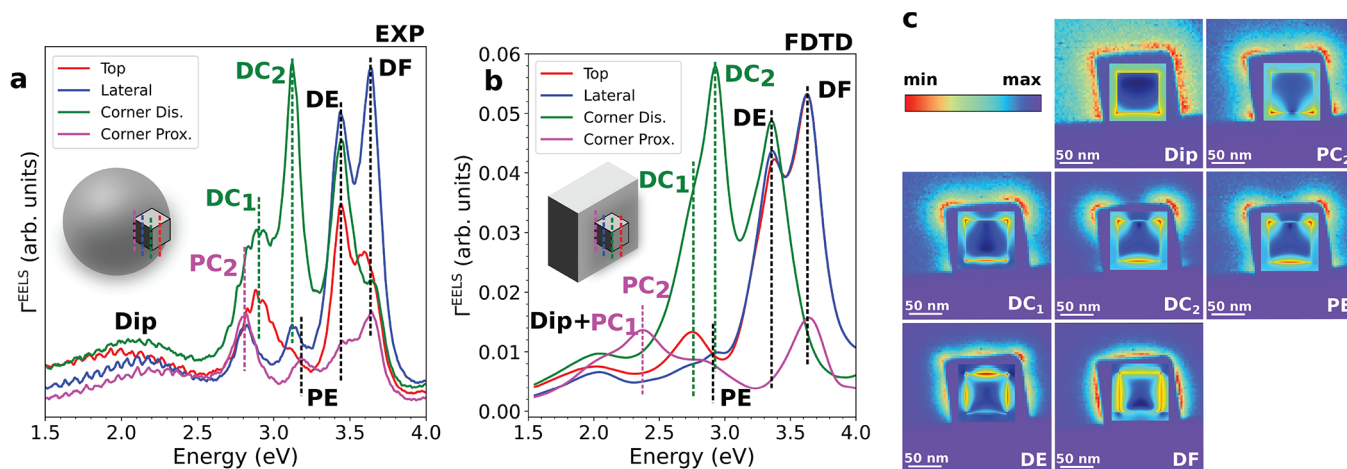


**Figure 3.** Characterization of MNP-WGMR coupling. (a) Experimental electron energy-loss spectra of a silver nanocube of  $\sim 105$  nm side length placed on a silica sphere for four different probe positions, as indicated by the inset scheme. (b) FDTD simulated electron energy-loss spectra of a 100 nm silver nanocube on a  $\text{SiO}_2$  planar substrate for similar probe positions. (c) Spectral maps obtained by EELS for all identified modes and, superimposed, the FDTD-simulated absolute value of the electric field.

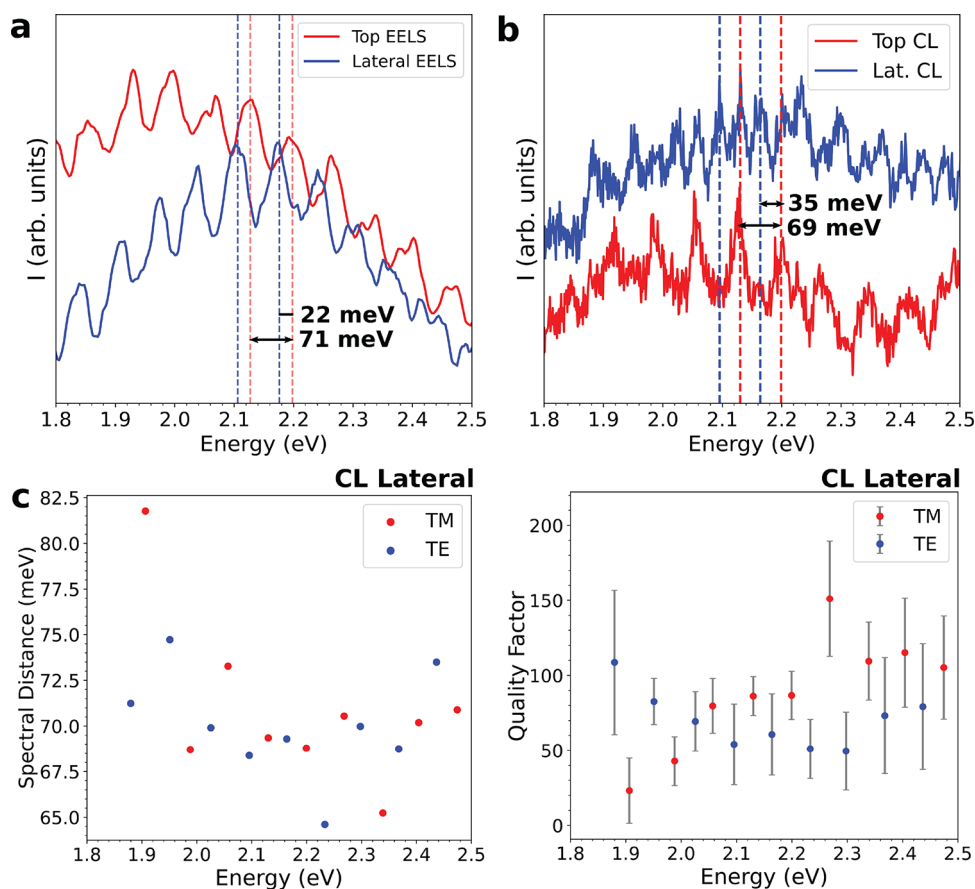


**Figure 4.** Polarization dependence of the NMP-WGMR coupling. (a, b) Polarization dependence on the probe position as observed in the EELS (a) and CL (b) signals associated with the dipolar mode. TM and TE modes are simultaneously observed in CL for the lateral probe position, while they are unobservable in EELS due to the limited spectral resolution of the electron source. (c) Spectral distance and quality factors for the resonances found with the lateral probe position. The uncertainty in the spectral distance is  $< 1$  meV for all data points.

beam undermine mode order identification and the estimation of the index of refraction (see the [Supporting Information](#) for further details). The  $Q$  factors from FDTD follow an exponential-like profile, as radiation leakage is the only source of loss in the simulation. The inflection point near 2.8 eV in the experimental  $Q$  factor from CL can be attributed to a

combination of experimentally induced losses, such as the effect of the carbon membrane and surface inhomogeneities<sup>61,63</sup> as well as the expected quality factor reduction from the increased radial order.

To study the coupling of nanoparticles with WGMRs, we have drop-casted silver nanocubes of  $\sim 100$ – $120$  nm in side

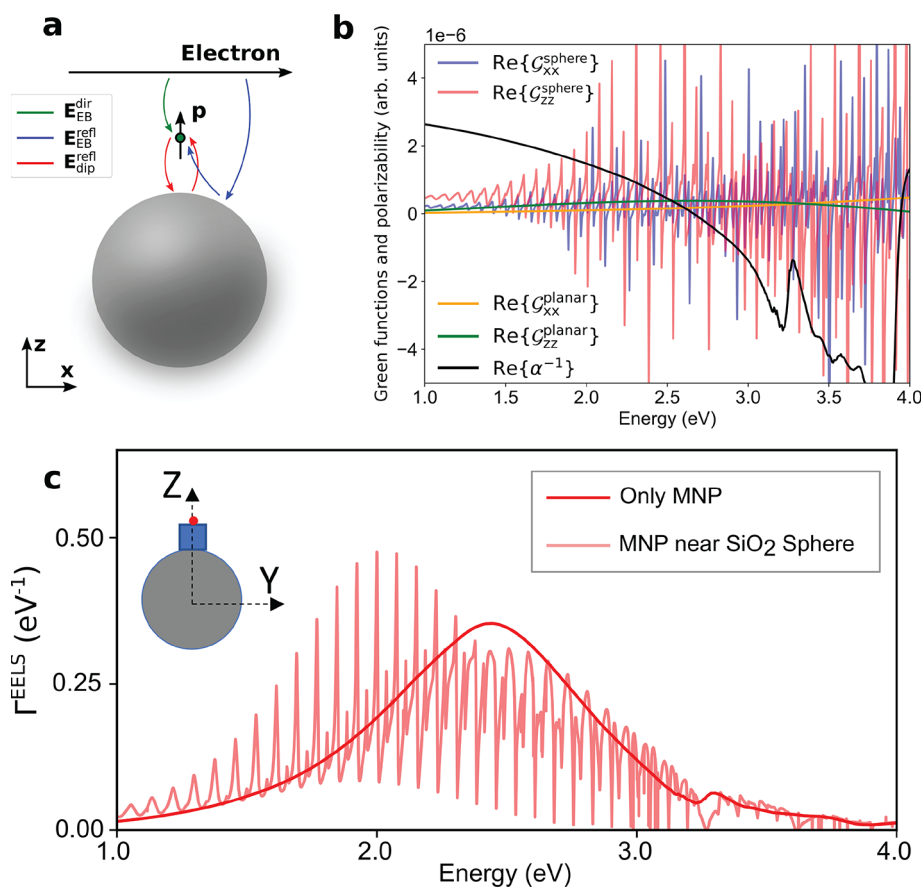


**Figure 5.** Analytical description of free-electron interaction with a MNP–WGMR hybrid system. (a) Electric field contributions to the self-consistent dipole model (see main text), where the MNP is treated as a dipolar scatterer. (b) Calculated electromagnetic Green tensor components for the self-induced field produced by the particle dipole on itself due to the presence of the dielectric sphere, in comparison with the real part of the inverse of the MNP polarizability. (c) Model calculation of the EELS probability corresponding to the nanocube alone and the nanocube placed near the sphere for the electron beam position shown in the inset.

length, synthesized by seed-mediated growth<sup>64,65</sup> in the sample grid containing the  $\text{SiO}_2$  spheres. To mitigate the direct coupling of the electron beam with the WGMR, the electron acceleration is kept at 100 keV, where the coupling terms for angular modes  $l \approx 20$  are reduced by 2 orders of magnitude (see the Supporting Information). In theory, bare nanocubes are known to support an infinite number of optical modes,<sup>66,67</sup> which are conventionally divided into corner (C), edge (E), and face (F) modes.<sup>68–71</sup> The presence of the  $\text{SiO}_2$  sphere, as a substrate, induces mode hybridization for each of the C, E, and F modes, leading to the so-called proximal and distal splitting in reference to the induced fields concentrated close or opposite to the substrate,<sup>72,73</sup> respectively. Figure 3 shows the most notable of these modes identified simultaneously by EELS and FDTD simulations, done by placing a 100 nm Ag nanocube on a 500 nm thick  $\text{SiO}_2$  plane substrate in order to observe the cube–substrate hybridization. Weak coupling between the gallery modes circulating in the sphere and the cube surface plasmons is observed in the spectral range of the dipolar mode (Dip) and, to a lesser extent, in the first observed distal corner ( $\text{DC}_1$ ) resonance, as shown in Figure 3a.

Loss spectra were studied with the electron probe positioned at the cube top (opposite edge from the substrate), side (lateral edge), distal corner (opposite corner from substrate), and proximal corner (closer corner to substrate) positions, which contain all possible symmetries of the problem. No gallery modes were observed in the proximal corner mode  $\text{PC}_2$ ,

the second distal corner  $\text{DC}_2$ , the proximal and distal edge modes (PE and DE, respectively), and the distal face mode DF, even though similar bare resonators exhibited detectable modes of up to 7 eV under 200 keV electron excitation. This behavior can be attributed to the near-zero net dipole moment of these higher-order modes, and thus, the resulting electric field is not enough to be observed in the EELS spectrum. Figure 3c shows filtered spectral maps of the cube modes, which match the already-known tomographic reconstructions of this system<sup>73</sup> and were also observed in the FDTD simulations. The absolute value of the electric field obtained from FDTD for each of the cube modes is shown in the respective experimental cube map. Finally, we have performed FDTD simulations of an entire spectral image that confirm the observed spatial and spectral features of the nanocube (see the Supporting Information).

Due to the much more complex distribution of the local electric field associated with these higher-order modes, we have focused our analysis on the dipolar mode (Dip) of the cube, which is characterized by dipole moments along the three main symmetry directions. Within the dipolar picture, we suggest that different probe positions induce different gallery-mode polarizations that translate into net dipolar moment directions. As TE modes have no radial electric fields ( $\mathbf{r} \cdot \mathbf{E} = 0$ ), the top probe position primarily excites TM modes. If the probe is placed laterally with respect to the cube, the resulting electric field is mostly tangential to the sphere surface and can thus

excite both TE and TM modes.<sup>34,74</sup> The experimental results from EELS show resonances that are equally spaced by  $\sim 71$  meV for each top and lateral probe position, but shifted  $\sim 22$  meV between each other, as shown in Figure 4. This value is smaller than the fwhm derived from the EELS spectra and therefore limits the resolution of possible neighboring TE and TM resonances. CL offers a simple solution to further explore the problem, thanks to its superior spectral resolution.

The employed CL system is angle-selective and can only detect gallery modes that circulate close to the plane containing the electron trajectory due to the mirror position relative to the sample and the electron beam direction. Experimental CL results are shown in Figure 4b. For the top probe position, which induces a strong radial electric field, TM polarization is more clearly resolved, while for a lateral probe, both sets of TM and TE resonances can be observed. The measured FSR is  $\sim 69$  meV, and the TE-TM spectral distance can be directly determined with the lateral probe spectrum as  $\sim 35$  meV.

We have fitted the resonances measured in the lateral probe position and divided them into two different sets. Consecutive modes were subtracted to obtain a spectral distance curve, and the standard deviation was used to estimate  $Q$  factors. We have also included error bars for the  $Q$  factors due to the non-negligible fitting uncertainties. The spectral distance curve shows no notable difference between polarizations, as expected from its definition. The  $Q$  factor for TE modes has a minimum value centered at the cube dipole resonance, which is expected because cube-induced losses are then maximal. For the TM modes, we observed a steady  $Q$  factor decrease down to the lowest energy resonance at  $\sim 1.9$  eV, but not a clear minimum. Unfortunately, the low emitted light intensity and the impossibility of easily changing the electron acceleration preclude further exploration of the coupled system.

It is worth mentioning that CL results outside the dipolar energy range were also obtained. While induced gallery modes were not observed in EELS for DC<sub>2</sub> (Figure 3a), CL clearly displays a coupling component (Figure S5 in the Supporting Information). This observation reinforces the argument that the coupling strength is dependent on the net dipole moment. Since CL measures the radiative component of the coupled plasmon-WGM mode, induced gallery modes can be observed. In addition, EELS is a combination of radiative and nonradiative losses and, because the nonradiative contribution only contains plasmonic losses and dominates over the radiative component, gallery modes are difficult to resolve in the EELS spectra.

To obtain further insight into the physics of the nanocube-sphere system, we have developed a semianalytical model that captures the main elements of the experiment. In this model, the MNP is described as a dipolar scatterer of polarizability  $\alpha(\omega)$  whose dielectric environment is modified by the presence of the dielectric sphere. The latter enters through a  $3 \times 3$  Green tensor  $\mathcal{G}$  that transforms the effective particle polarizability into  $\alpha^{\text{eff}} = 1/(\alpha^{-1} - \mathcal{G})$ , and whose components are obtained from the electric field induced at the position of a unit dipole placed at the nanocube center. We calculate  $\alpha(\omega)$  from a finite-difference method (see Figure S6 in the Supporting Information) and  $\mathcal{G}$  using the boundary-element method<sup>46</sup> in the presence of the sphere.

These elements are represented in Figure 5b, where  $\text{Re}\{\alpha^{-1}\}$  is found to change sign around 2.5 eV, indicating the

emergence of a prominent particle plasmon, whereas  $\mathcal{G}$  displays sharp oscillations revealing the effect of coupling to the Mie modes of the sphere. For comparison, we show  $\mathcal{G}$  for a planar silica surface, which shows a featureless profile. From these considerations, we understand that we are in the weak-coupling regime because the lifetime of the MNP dipole is much smaller than that of the whispering-gallery modes, so that the imaginary part in the denominator of  $\alpha^{\text{eff}}$  remains relatively large and is dominated by the nanocube component. Then, the optical response of the MNP-sphere hybrid system is enhanced at the points in which the real part of the denominator is canceled, as indicated by the crossings between  $\text{Re}\{\alpha^{-1}\}$  and  $\text{Re}\{\mathcal{G}\}$  in Figure 5b. The effective dipole induced on the particle receives contributions associated with different scattering paths, as schematically shown in Figure 5a. Namely, it is contributed by the direct field produced by the electron ( $E_{\text{EB}}^{\text{dir}}$ ), as well as by the scattering of this field at the sphere ( $E_{\text{EB}}^{\text{eff}}$ ) and the scattering of the dipole field at the sphere acting back on the dipole ( $E_{\text{dip}}^{\text{refl}}$ ); these contributions are all captured in  $\alpha^{\text{eff}}$ , from which a scattering series can directly be constructed by a Taylor expansion in powers of  $\alpha\mathcal{G}$ .

To calculate EELS in this analytical model, we use the multiple elastic scattering of multipole expansions (MESME) method<sup>75</sup> with the sphere and the MNP acting as scattering centers. In particular, the sphere is described by multipoles up to an order of  $>30$  and the MNP through the electric dipolar components of the scattering matrix. This method captures all scattering paths schematically represented in Figure 5a. The results presented in Figure 5c confirm the analysis based on  $\alpha^{\text{eff}}$ : the EELS probability with the MNP alone exhibits a prominent plasmon, but it is modulated through coupling to Mie resonances of the sphere in a way similar to that observed in experiment. Note that the model successfully describes the sphere and MNP coupling within the dipolar picture, but it does not account for higher-order plasmon modes. In this sense, although Figure 5 shows gallery modes along the entire displayed energy range, they are not observed in Figure 3a because higher-order modes mask the tail of the dipolar resonance. Further discussion of the analytical model can be found in the Supporting Information.

In conclusion, we have described, with high spatial resolution, the coupling of MNPs to WGMRs using fast electrons, observed from both energy absorption (EELS) and light emission (CL) measurements. While CL can be used to improve the experimental spectral resolution, EELS provides rich and complete absorption information over a large spectral range: a compelling example on how EELS and CL can be used together to provide self-complementary information. The combined EELS-CL measurements would be even more relevant if the electron energy could be changed without causing major microscope misalignment. Beyond its remarkable agreement with experiments, FDTD-simulated energy-loss spectroscopy provides us with a deep physical insight into the coupling mechanism. Finally, the plasmon resonance excitation by the electron probe allows for the manipulation of the gallery-mode polarization by either coupling to TM or to both TM and TE resonances. With the advent of a new generation of monochromated STEMs, experiments requiring such high spectral and spatial resolution are now possible. With this work, we help to open a path for high-quality-factor and small-modal-volume photonic devices to be scrutinized in a STEM.

## ■ ASSOCIATED CONTENT

### SI Supporting Information

The Supporting Information is available free of charge at <https://pubs.acs.org/doi/10.1021/acs.nanolett.1c03826>.

Details on the electron coupling probability for bare WGMRs, fitting results for bare SiO<sub>2</sub> spheres, FDTD simulations for the hybridization of cube modes on a flat SiO<sub>2</sub> substrate, CL results for nondipolar modes in the WGM–plasmon coupled system, theoretical details of the metallic nanoparticle polarizability, and additional results from the analytical model (PDF)

## ■ AUTHOR INFORMATION

### Corresponding Authors

Yves Auad – *Laboratoire des Physique des Solides, Université Paris Saclay, CNRS, 91405 Orsay, France;*

Email: [yves.maia-auad@universite-paris-saclay.fr](mailto:yves.maia-auad@universite-paris-saclay.fr)

Mathieu Kociak – *Laboratoire des Physique des Solides, Université Paris Saclay, CNRS, 91405 Orsay, France;*

[orcid.org/0000-0001-8858-0449](https://orcid.org/0000-0001-8858-0449);

Email: [mathieu.kociak@universite-paris-saclay.fr](mailto:mathieu.kociak@universite-paris-saclay.fr)

### Authors

Cyrille Hamon – *Laboratoire des Physique des Solides, Université Paris Saclay, CNRS, 91405 Orsay, France;*

[orcid.org/0000-0001-9529-9102](https://orcid.org/0000-0001-9529-9102)

Marcel Tencé – *Laboratoire des Physique des Solides, Université Paris Saclay, CNRS, 91405 Orsay, France*

Hugo Lourenço-Martins – *Max Planck Institute for Biophysical Chemistry, 37077 Göttingen, Germany; IV. Physical Institute, University of Göttingen, 37077 Göttingen, Germany*

Vahagn Mkhitarian – *ICFO-Institut de Ciències Fotoniques, The Barcelona Institute of Science and Technology, 08860 Castelldefels (Barcelona), Spain*

Odile Stéphan – *Laboratoire des Physique des Solides, Université Paris Saclay, CNRS, 91405 Orsay, France*

F. Javier García de Abajo – *ICFO-Institut de Ciències Fotoniques, The Barcelona Institute of Science and Technology, 08860 Castelldefels (Barcelona), Spain; ICREA-Institució Catalana de Recerca i Estudis Avançats, 08010 Barcelona, Spain;* [orcid.org/0000-0002-4970-4565](https://orcid.org/0000-0002-4970-4565)

Luiz H. G. Tizei – *Laboratoire des Physique des Solides, Université Paris Saclay, CNRS, 91405 Orsay, France;*

[orcid.org/0000-0003-3998-9912](https://orcid.org/0000-0003-3998-9912)

Complete contact information is available at:

<https://pubs.acs.org/doi/10.1021/acs.nanolett.1c03826>

### Notes

The authors declare the following competing financial interest(s): M.K. patented and licensed technologies concerning the Attolight Mönch CL system and is a part-time consultant for this company. All other authors declare no competing financial interests.

## ■ ACKNOWLEDGMENTS

The present project has been funded partially by the National Agency for Research under the program of future investment TEMPOS-CHROMATEM (reference no. ANR-10-EQPX-50), by the European Union's Horizon 2020 research and innovation programme under grant agreement Nos. 823717 (ESTEEM3) and 101017720 (EBEAM), and by the French

National Research Agency (QUENOT ANR-20-CE30-0033). V.M. and F.J.G.d.A. acknowledge support from the European Research Council (Advanced Grant No. 789104eNANO), Spanish MCINN (PID2020-112625GB-I00 and CEX2019-000910-S), Generalitat de Catalunya (CERCA and AGAUR), and Fundació Cellex and Mir-Puig.

## ■ REFERENCES

- (1) Link, S.; El-Sayed, M. Shape and Size Dependence of Radiative, Non-Radiative and Photothermal Properties of Gold Nanocrystals. *Int. Rev. Phys. Chem.* **2000**, *19*, 409–453.
- (2) Tian, Z.; Ren, B.; Wu, D. Surface-Enhanced Raman Scattering: From Noble to Transition Metals and from Rough Surfaces to Ordered Nanostructures. *J. Phys. Chem. B* **2002**, *106*, 9463–9483.
- (3) Sun, Y.; Xia, Y. Gold and silver nanoparticles: A class of chromophores with colors tunable in the range from 400 to 750 nm. *Analyst* **2003**, *128*, 686–691.
- (4) Liz-Marzán; Nanometals, L. Formation and color. *Mater. Today* **2004**, *7*, 26–31.
- (5) Vahala, K. Optical Microcavities. *Nature* **2003**, *424*, 839–846.
- (6) Vernooij, D.; Furusawa, A.; Georgiades, N.; Ilchenko, V.; Kimble, H. Cavity QED with high-Q whispering gallery modes. *Phys. Rev. A* **1998**, *57*, R2293.
- (7) Wiederhecker, G.; Chen, L.; Gondarenko, A.; Lipson, M. Controlling photonic structures using optical forces. *Nature* **2009**, *462*, 633–636.
- (8) Kippenberg, T.; Rokhsari, H.; Carmon, T.; Scherer, A.; Vahala, K. Analysis of Radiation-Pressure Induced Mechanical Oscillation of an Optical Microcavity. *Phys. Rev. Lett.* **2005**, *95*, 033901.
- (9) Zhu, J.; Ozdemir, S.; Xiao, Y.; Li, L.; He, L.; Chen, D.; Yang, L. On-chip single nanoparticle detection and sizing by mode splitting in an ultrahigh-Q microresonator. *Nat. Photonics* **2010**, *4*, 46–49.
- (10) Zheng, Y.; Wu, Z.; Shum, P.; Xu, Z.; Humbert, G.; Zhang, H.; Zeng, S.; Dinh, X. Sensing and lasing applications of whispering gallery mode microresonators. *Opto-Electronic Adv.* **2018**, *1*, 18001501.
- (11) Rayleigh, L. CXII. The problem of the whispering gallery. *Philosoph. Magaz. Ser. 6* **1910**, *20*, 1001–1004.
- (12) Knight, J.; Cheung, G.; Jacques, F.; Birks, T. Phase-Matched Excitation of Whispering-Gallery-Mode Resonances by a Fiber Taper. *Opt. Lett.* **1997**, *22*, 1129–1131.
- (13) Braginsky, V.; Gorodetsky, M.; Ilchenko, V. Quality-factor and nonlinear properties of optical whispering-gallery modes. *Phys. Lett. A* **1989**, *137*, 393–397.
- (14) Cai, M.; Painter, O.; Vahala, K. Observation of Critical Coupling in a Fiber Taper to a Silica-Microsphere Whispering-Gallery Mode System. *Phys. Rev. Lett.* **2000**, *85*, 74.
- (15) Nussenzveig, H. M. Diffraction Effects in Semiclassical Scattering; *Montrroll Memorial Lecture Series in Mathematical Physics*; Cambridge University Press: 1992.
- (16) Matsko, A.; Ilchenko, V. Optical Resonators With Whispering-Gallery Mode-Part I. *IEEE J. Sel. Top. Quantum Electron.* **2006**, *12*, 3–14.
- (17) Miri, N.; Mohammadzakeri, M. Optical Sensing Using Microspheres With Different Size and Material. *IEEE Sens. J.* **2014**, *14*, 3593–3598.
- (18) Liu, C.; Di Falco, A.; Molinari, D.; Khan, Y.; Ooi, B.; Krauss, T.; Fratalocchi, A. Enhanced energy storage in chaotic optical resonators. *Nat. Photonics* **2013**, *7*, 473–478.
- (19) Lacey, S.; Wang, H. Directional emission from whispering-gallery modes in deformed fused-silica microspheres. *Opt. Lett.* **2001**, *26*, 1943–1945.
- (20) Kippenberg, T.; Tchebotareva, A.; Kalkman, J.; Polman, A.; Vahala, K. Purcell-Factor-Enhanced Scattering from Si Nanocrystals in an Optical Microcavity. *Phys. Rev. Lett.* **2009**, *103*, 027406.
- (21) Motsch, M.; Zeppenfeld, M.; Pinkse, P.; Rempe, G. Cavity-Enhanced Rayleigh Scattering. *New J. Phys.* **2010**, *12*, 063022.

- (22) Mazzei, A.; Göttinger, S.; Menezes, L.; Zumofen, G.; Benson, O.; Sandoghdar, V. Controlled Coupling of Counterpropagating Whispering-Gallery Modes by a Single Rayleigh Scatterer: A Classical Problem in a Quantum Optical Light. *Phys. Rev. Lett.* **2007**, *99*, 173603.
- (23) Zhi, Y.; Valenta, J.; Meldrum, A. Structure of whispering gallery mode spectrum of microspheres coated with fluorescent silicon quantum dots. *J. Opt. Soc. Am. B* **2013**, *30*, 3079–3085.
- (24) Vollmer, F.; Braun, D.; Libchaber, A.; Khoshima, M.; Teraoka, I.; Arnold, S. Protein Detection by Optical Shift of a Resonant Microcavity. *Appl. Phys. Lett.* **2002**, *80*, 4057–4059.
- (25) Zhi, Y.; Yu, X.; Gong, Q.; Yang, L.; Xiao, Y. Single Nanoparticle Detection Using Optical Microcavities. *Adv. Mater.* **2017**, *29*, 1604920.
- (26) Vollmer, F.; Arnold, S.; Keng, D. Single virus detection from the reactive shift of a whispering-gallery mode. *Proc. Natl. Acad. Sci. U. S. A.* **2008**, *105*, 20701–20704.
- (27) Weiss, D.; Sandoghdar, V.; Hare, J.; Lefèvre-Seguin, V.; Raimond, J.; Haroche, S. Splitting of high-Q Mie modes induced by light backscattering in silica microspheres. *Opt. Lett.* **1995**, *20*, 1835–1837.
- (28) Ozdemir, S.; Zhu, J.; He, L.; Yang, L. Estimation of Purcell factor from mode-splitting spectra in an optical microcavity. *Phys. Rev. A: At., Mol., Opt. Phys.* **2011**, *83*, 033817.
- (29) Shen, B.; Yu, X.; Zhi, Y.; Wang, L.; Kim, D.; Gong, Q.; Xiao, Y. Detection of single nanoparticles using the dissipative interaction in a high-Q microcavity. *Phys. Rev. Appl.* **2016**, *5*, 024011.
- (30) Shao, L.; Jiang, X.; Yu, X.; Li, B.; Clements, W.; Vollmer, F.; Wang, W.; Xiao, Y.; Gong, Q. Detection of Single Nanoparticles and Lentiviruses Using Microcavity Resonance Broadening. *Adv. Mater.* **2013**, *25*, 5616–5620.
- (31) Zhang, J.; Jin, X.; Morales-Guzman, P.; Liu, H.; Zhang, H.; Razzari, L.; Claverie, J. Engineering the Absorption and Field Enhancement Properties of Au-TiO<sub>2</sub> Nanohybrids via Whispering Gallery Mode Resonances for Photocatalytic Water Splitting. *ACS Nano* **2016**, *10*, 4496–4503.
- (32) Tong, L.; Wang, P.; Wang, Y.; Yang, Z.; Guo, X.; Lin, X.; Yu, X.; Xiao, Y.; Fang, W.; Zhang, L.; Lu, G.; Gong, Q. Single-Band 2-nm-Line-Width Plasmon Resonance in a Strongly Coupled Au Nanorod. *Nano Lett.* **2015**, *15*, 7581–7586.
- (33) Ai, Q.; Gui, L.; Paone, D.; Metzger, B.; Mayer, M.; Weber, K.; Fery, A.; Giessen, H. Ultranarrow Second-Harmonic Resonances in Hybrid Plasmon-Fiber Cavities. *Nano Lett.* **2018**, *18*, 5576–5582.
- (34) Gu, F.; Zhang, L.; Zhu, Y.; Zeng, H. Free-space coupling of nanoantennas and whispering-gallery microcavities with narrowed linewidth and enhanced sensitivity. *Laser & Photonics Review* **2015**, *9*, 682–688.
- (35) Kociak, M.; Stéphan, O. Mapping Plasmons at the Nanometer Scale in an Electron Microscope. *Chem. Soc. Rev.* **2014**, *43*, 3865–3883.
- (36) Yamamoto, N.; Araya, K.; García de Abajo, F. J. Photon emission from silver particles induced by a high-energy electron beam. *Phys. Rev. B: Condens. Matter Mater. Phys.* **2001**, *64*, 205419.
- (37) Kociak, M.; Zagonel, L. Cathodoluminescence in the scanning transmission electron microscope. *Ultramicroscopy* **2017**, *176*, 112–131.
- (38) Hyun, J.; Couillard, M.; Rajendran, P.; Liddell, C.; Muller, D. Measuring far-ultraviolet whispering gallery modes with high energy electrons. *Appl. Phys. Lett.* **2008**, *93*, 243106–243106.
- (39) Barwick, B.; Flannigan, D.; Zewail, A. Photon-induced near-field electron microscopy. *Nature* **2009**, *462*, 902–906.
- (40) Kfir, O.; Lourenço-Martins, H.; Storeck, G.; Sivilis, M.; Harvey, T.; Kippenberg, T.; Feist, A.; Ropers, C. Controlling free electrons with optical whispering-gallery modes. *Nature* **2020**, *582*, 46–49.
- (41) Müller, N.; Hock, V.; Koch, H.; Bach, N.; Rathje, C.; Schäfer, S. Broadband Coupling of Fast Electrons to High-Q Whispering-Gallery Mode Resonators. *ACS Photonics* **2021**, *8*, 1569–1575.
- (42) Rossouw, D.; Couillard, M.; Vickery, J.; Kumacheva, E.; Botton, G. Multipolar Plasmon Resonances in Silver Nanowire Antennas Imaged with a Subnanometer Electron Probe. *Nano Lett.* **2011**, *11*, 1499–1504.
- (43) Kociak, M.; Nelayah, J.; Stéphan, O.; Mazzucco, S.; García de Abajo, F. J.; Bernard, R.; Colliex, C. Mapping Surface Plasmons on a Single Metallic Nanoparticle. *Nat. Phys.* **2008**, *3*, MMC1.
- (44) García de Abajo, F. J. Relativistic energy loss and induced photon emission in the interaction of a dielectric sphere with an external electron beam. *Phys. Rev. B: Condens. Matter Mater. Phys.* **1999**, *59*, 3095.
- (45) García de Abajo, F. J. Multiple scattering of radiation in clusters of dielectrics. *Phys. Rev. B: Condens. Matter Mater. Phys.* **1999**, *60*, 6086.
- (46) García de Abajo, F. J. Optical excitations in electron microscopy. *Rev. Mod. Phys.* **2010**, *82*, 209–275.
- (47) Hulst, H. Optics of Spherical Particles. *Recherches Astronomiques de l'Observatoire d'Utrecht* **1946**, *11*, 1.
- (48) Stratton, J. *Electromagnetic Theory*; McGraw-Hill: 1941.
- (49) Mie, G. Beiträge zur Optik Trüber Medien, Speziell Kolloidaler Metallösungen. *Ann. Phys.* **1908**, *330*, 377.
- (50) Losquin, A.; Zagonel, L. F.; Myroshnychenko, V.; Rodríguez-González, B.; Tencé, M.; Scarabelli, L.; Förstner, J.; Liz-Marzán, L. M.; García De Abajo, F. J.; Stéphan, O.; Kociak, M. Unveiling nanometer scale extinction and scattering phenomena through combined electron energy loss spectroscopy and cathodoluminescence measurements. *Nano Lett.* **2015**, *15*, 1229–1237.
- (51) Non-functionalized Silica. 2020; <https://bangslabs.com>, Accessed on 08.12.2021.
- (52) Krivanek, O. L.; Lovejoy, T. C.; Dellby, N.; Aoki, T.; Carpenter, R. W.; Rez, P.; Soignard, E.; Zhu, J.; Batson, P. E.; Lagos, M. J.; Egerton, R. F.; Crozier, P. A. Vibrational spectroscopy in the electron microscope. *Nature* **2014**, *514*, 209–212.
- (53) Hachtel, J. A.; Huang, J.; Popovs, I.; Jansone-Popova, S.; Keum, J. K.; Jakowski, J.; Lovejoy, T. C.; Dellby, N.; Krivanek, O. L.; Idrobo, J. C. Identification of site-specific isotopic labels by vibrational spectroscopy in the electron microscope. *Science* **2019**, *363*, 525–528.
- (54) Hage, F. S.; Radtke, G.; Kepaptsoglou, D. M.; Lazzeri, M.; Ramasse, Q. M. Single-atom vibrational spectroscopy in the scanning transmission electron microscope. *Science* **2020**, *367*, 1124–1127.
- (55) Tizei, L. H. G.; et al. Tailored Nanoscale Plasmon-Enhanced Vibrational Electron Spectroscopy. *Nano Lett.* **2020**, *20*, 2973–2979.
- (56) Mkhitarian, V.; March, K.; Tseng, E. N.; Li, X.; Scarabelli, L.; Liz-Marzán, L. M.; Chen, S.-Y.; Tizei, L. H. G.; Stéphan, O.; Song, J.-M.; Kociak, M.; García de Abajo, F. J.; Gloter, A. Can Copper Nanostructures Sustain High-Quality Plasmons? *Nano Lett.* **2021**, *21*, 2444–2452.
- (57) Lumerical 2020 R2. 2020; <https://lumerical.com>, Accessed on 08.12.2021.
- (58) Cao, Y.; Manjavacas, A.; Large, N.; Nordlander, P. Electron Energy-Loss Spectroscopy Calculation in Finite-Difference Time-Domain Package. *ACS Photonics* **2015**, *2*, 369–375.
- (59) Sumlin, B. *PyMieScatt: Release v1.8.1*, 2020; <https://pymiescatt.readthedocs.io>, Accessed on 08.12.2021.
- (60) Malitson, I. Interspecimen Comparison of the Refractive Index of Fused Silica. *J. Opt. Soc. Am.* **1965**, *55*, 1205–1208.
- (61) Righini, G.; Dumeige, Y.; Feron, P.; Ferrari, M.; Nunzi Conti, G.; Ristić, D.; Soria, S. Whispering Gallery Mode microresonators: Fundamentals and applications. *La Rivista del Nuovo Cimento* **2011**, *34*, 435.
- (62) Schunk, G.; Fürst, J.; Förtsch, M.; Strekalov, D.; Vogl, U.; Sedlmeir, F.; Schwefel, H.; Leuchs, G.; Marquardt, C. Identifying modes of large whispering-gallery mode resonators from the spectrum and emission pattern. *Opt. Express* **2014**, *22*, 30795–30806.
- (63) Buck, J.; Kimble, H. Optimal Sizes of Dielectric Microspheres for Cavity QED with Strong Coupling. *Phys. Review A* **2003**, *67*, 033806.
- (64) Zheng, Y.; Zhong, X.; Li, Z.; Xia, Y. Successive, Seed-Mediated Growth for the Synthesis of Single-Crystal Gold Nanospheres with Uniform Diameters Controlled in the Range of 5–150 nm. *Part. & Part. Systems Charact* **2014**, *31*, 266–273.

(65) Mayer, M.; Scarabelli, L.; March, K.; Altantzis, T.; Tebbe, M.; Kociak, M.; Bals, S.; García de Abajo, F. J.; Fery, A.; Liz-Marzán, L. Controlled Living Nanowire Growth: Precise Control over the Morphology and Optical Properties of AgAuAg Bimetallic Nanowires. *Nano Lett.* **2015**, *15*, 5427–5437.

(66) Fuchs, R. Theory of the optical properties of ionic crystal cubes. *Phys. Rev. B* **1975**, *11*, 1732.

(67) Langbein, D. Normal modes at small cubes and rectangular particles. *J. Phys. A: Math. Gen.* **1976**, *9*, 627.

(68) Sherry, L.; Chang, S.; Schatz, G.; Duyne, R.; Wiley, B.; Xia, Y. Localized Surface Plasmon Resonance Spectroscopy of Single Silver Nanocubes. *Nano Lett.* **2005**, *5*, 2034–2038.

(69) Mazzucco, S.; Geuquet, N.; Ye, J.; Stéphan, O.; Roy, W.; Van Dorpe, P.; Henrard, L.; Kociak, M. Ultralocal Modification of Surface Plasmons Properties in Silver Nanocubes. *Nano Lett.* **2012**, *12*, 1288–1294.

(70) Li, X.; Haberer, G.; Hohenester, U.; Stéphan, O.; Kothleitner, G.; Kociak, M. Three-dimensional vectorial imaging of surface phonon polaritons. *Science* **2021**, *371*, 1364–1367.

(71) Lourenço-Martins, H.; Kociak, M. Vibrational surface electron-energy-loss spectroscopy probes confined surface-phonon modes. *Phys. Rev. X* **2017**, *7*, 1–11.

(72) Zhang, S.; Bao, K.; Halas, N.; Xu, H.; Nordlander, P. Substrate-Induced Fano Resonances of a Plasmonic Nanocube: A Route to Increased-Sensitivity Localized Surface Plasmon Resonance Sensors Revealed. *Nano Lett.* **2011**, *11*, 1657–1663.

(73) Nicoletti, O.; Peña, F.; Leary, R.; Holland, D.; Ducati, C.; Midgley, P. Three-dimensional imaging of localized surface plasmon resonances of metal nanoparticles. *Nature* **2013**, *502*, 80–84.

(74) Hall, J.; Afshar, S.; Henderson, M.; Francois, A.; Reynolds, T.; Riesen, N.; Monro, T. Method for predicting whispering gallery mode spectra of spherical microresonators. *Opt. Expr.* **2015**, *23*, 9924–9937.

(75) García de Abajo, F. J. Relativistic description of valence energy losses in the interaction of fast electrons with clusters of dielectrics: multiple-scattering approach. *Phys. Rev. B: Condens. Matter Mater. Phys.* **1999**, *60*, 6103–6112.